Substrate Phonon-Mediated Plasmon Hybridization in Coplanar Graphene Nanostructures for Broadband Plasmonic Circuits

Xiaoxia Yang, Xiang-Tian Kong, Bing Bai, Zhenjun Li, Hai Hu, Xiaohui Qiu, and Qing Dai**

The mode hybridization between adjacent graphene nanoribbons determines the integration density of graphene-based plasmonic devices. Here, plasmon hybridization in graphene nanostructures is demonstrated through the characterization of the coupling strength of plasmons in graphene nanoribbons as a function of charge density and inter-ribbon spacing using Fourier transform infrared microscopy. In combination with numerical simulations, it is shown that the plasmon coupling is strongly mediated by the substrate phonons. For polar substrates, the plasmon coupling strength is limited by the plasmon–phonon interactions. In contrast, a nonpolar substrate affects neither the energy distribution of the original plasmon modes in graphene nanostructures nor their plasmon interactions, which increases exponentially as the inter-ribbon spacing decreases. To further explore the potential of graphene broadband plasmonics on nonpolar substrates, a scheme is proposed that uses a metal–dielectric heterostructure to prevent the overlap of plasmons between neighboring graphene nanoribbons. The device structures retain the plasmon resonance frequency of the graphene ribbons and maximally isolate the plasmonic components from the surrounding electromagnetic environment, allowing modular design in integrated plasmonic circuits.

1. Introduction

Graphene holds great promise for applications in photonics and optoelectronics owing to its ability to support terahertz surface plasmons and electrically tunable optical conductivity.[1–3] The resonance frequency of the confined plasmons in micro/nano-structures of graphene can be controlled by adjusting the structural size[4–6] and the carrier density[3–10] of graphene, enabling actively controlled plasmonic devices.[3,6,8–12] Recent demonstrations, such as terahertz optical modulators,[4,13] nanoresonators[14] and broadband optoelectronic devices,[12,15] complementary to the extraordinary electrical properties of graphene, enable a scheme to construct one-atom-thick photonic integrated circuits based on graphene and its hybrid materials.[15,16]

The crosstalk of the operating modes in neighboring components is one of the primary concerns in the design and engineering of miniaturized plasmonic circuits.[17] This corresponds to the distance under which components can operate independently without modifying their intrinsic behaviors, particularly for subwavelength plamonic structures. To simulate the situation, several groups have investigated the excitation and propagation of plasmon resonances in prototype waveguides made of graphene micro/nano-ribbon arrays.[4,5,14,18–20] For example, Christensen et al. examined the interaction between plasmons in a pair of graphene nanoribbon in planar configuration using a classical electromagnetic model.[19] They found that the

Dr. X. Yang, Dr. X.-T. Kong, Dr. B. Bai,
Dr. Z. Li, H. Hu, Prof. X. Qiu, Prof. Q. Dai
National Center for Nanoscience and Technology
Beijing 100190, China
E-mail: xhqiu@nanoctr.cn; daiq@nanoctr.cn
DOI: 10.1002/smll.201400515

coupling of plasmons led to hybridized states, which sensitively depends on inter-ribbon distance. In a recent study by Strait et al., quantitative comparisons between the calculation and experimental results concluded that the hybridization among plasmon modes played an important role in shifting the resonance frequency of graphene structures.[20] Despite the evanescent nature of leaky plasmon waves, the interactions between plasmon modes in neighboring nano-ribbons have been investigated as a means for plasmon guiding, in analogy to that achieved in aligned metallic nanoparticles.[21] To our knowledge, the studies to date have focused primarily on the coupled plasmons in graphene nanostructures without the underlying substrate. To truly fulfill the role of graphene waveguides in subwavelength plasmonic circuits, the effect of mode hybridization of plasmon resonance subjected to vibration phonons of various substrates has to be further clarified. Specific geometric configurations must be chosen to optimize the spatial confinement of propagating plasmons in practical cases.

In this work, we investigated the plasmon hybridization in coplanar graphene nanoribbons in terms of varying carrier density and inter-ribbon spacing by far-field IR spectroscopy. We found that the coupling effect between nanoribbons was subjected to substrate phonons, which strongly reduced the plasmon interactions on polar substrate. In contrast, our full vector electromagnetic calculation showed that the plasmon coupling on nonpolar substrate is not significantly affected by its interaction with substrate phonons, thereby the coupling of neighboring plasmons becomes a dominant behavior in this scenario. The coupling strength increases significantly as the inter-ribbon spacing decreases, but is insensitive to the Fermi levels at a given gap-to-ribbon ratio. We further demonstrated that the plasmon hybridization can be screened by a metal-dielectric heterostructure environment, which retains the intrinsic resonance as that of the isolated nanoribbon.

2. Results and Discussion

Fourier transform infrared microscopy was used to measure the light transmittance of the back-gated graphene nanoribbon arrays (GNRAs) fabricated on SiO_2/Si substrates (see Experimental section), as schematically shown in **Figure 1**a. An atomic force microscopy (AFM) image of a GNRA sample is presented in the inset of Figure 1b. The quality of the GNRAs was further proved by Raman spectroscopy (see the supporting information). A typical gate-dependent resistance curve of the GNRAs is shown in Figure 1b. The device showed a charge neutral point (CNP) at the gate voltage (V_g) of 42 V, indicating that the graphene layer was hole-doped at zero gate voltage. The charge mobility was estimated to be ~900 $cm^2V^{-1}s^{-1}$ according to reference.[22]

Figure 2a shows the extinction spectra of GNRAs with varying Fermi level (E_F) of graphene. The extinction spectrum of the gated GNRA was obtained from $(1 - T/T_{CNP})$,[5] where T is the measured transmittance of GNRA, and T_{CNP} is the transmittance at the CNPs. Each extinction spectrum is characteristic of multiple resonance peaks whose intensities depend on the carrier density of graphene. The peaks were generally weak when GNRA was nearly neutral, i.e., when the Fermi level was closed to CNPs. When more carriers were injected to the graphene ribbons, the peaks became enhanced and shifted to higher frequencies. For example, the peak 3 shifted ~25 cm^{-1} (from 1240 cm^{-1} to 1265 cm^{-1}) when the Fermi level varied from –0.14 eV to –0.32 eV. According to reference[5], the peaks are originated from the interactions of the graphene plasmons with the surface optical phonons of SiO_2 substrate at 806 cm^{-1} and 1168 cm^{-1}.[5,23] The plasmon-phonon coupled modes can be described within the random phase approximation, which suggests that the coupling is strong even if the Fermi level is low.[24–26]

The resonance frequency extracted from the spectra in Figure 2a as a function of the Fermi level of graphene ribbons was plotted in Figure 2b. The plasmon resonance was significantly influenced by the two surface optical phonons of the SiO_2 substrate, labeled as ω_{sp1} and ω_{sp2}, respectively. When the plasmon is free from the substrate phonons, the resonance frequency would be scaled as $E_F^{1/2}$ (dashed grey line in Figure 2b), which is a direct consequence of the quantum relativistic nature of the Dirac-Fermions in graphene.[4,24] In contrast, the plasmons resonances hybridized with the two

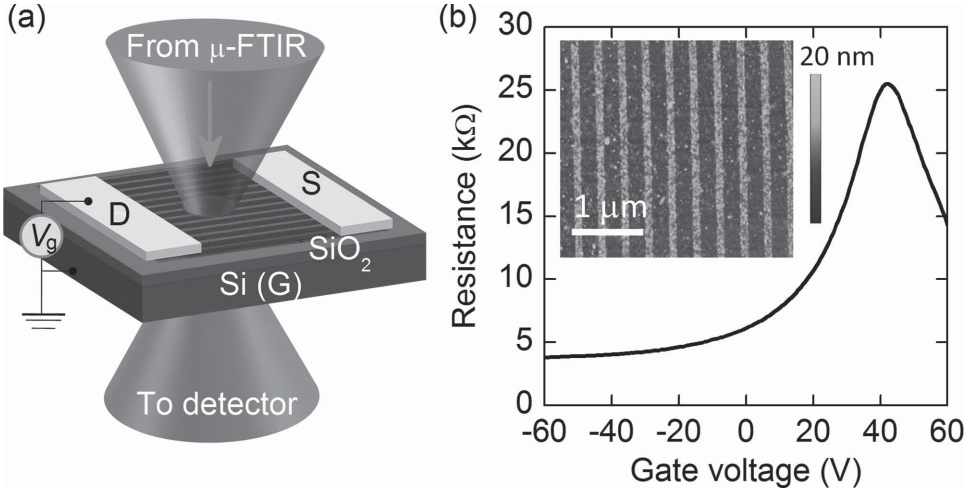

Figure 1. (a) Schematic diagram for detecting the extinction spectra of back-gated GNRAs by using Fourier transform infrared microscopy. (b) Gate-dependent resistance of a typical graphene nanoribbon array. Inset: AFM image of a GNRA with width of 140 nm and inter-ribbon spacing of 210 nm.

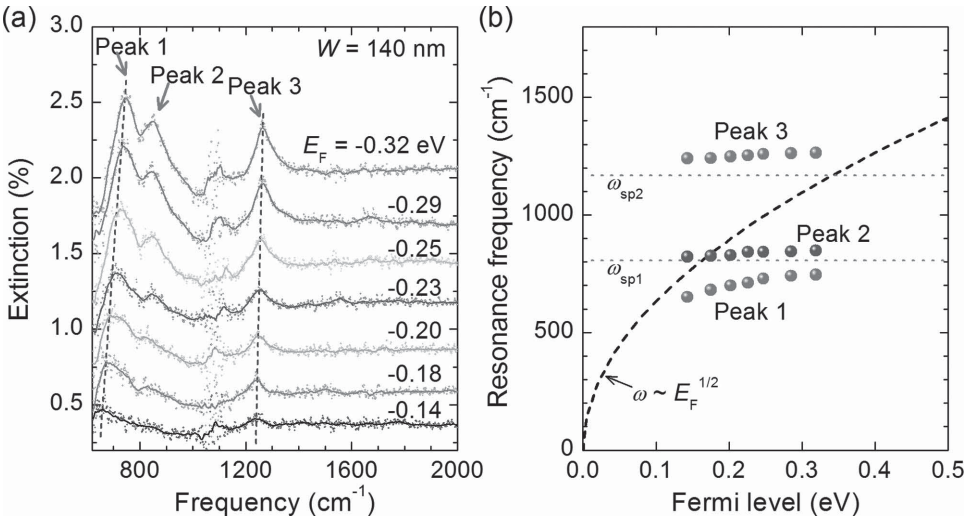

Figure 2. (a) Extinction spectra of GNRAs on SiO_2 as a function of the Fermi level of graphene. The Fermi level position of graphene at different biased voltage was determined via a capacitor model after the CNPs were obtained.[22] The ribbon width is 140 nm and the fraction of the array period occupied by graphene ribbon (filling factor) is 0.6. (b) Plasmon resonance affected by substrate phonons. Circles are the resonance frequency extracted from (a) as a function of the Fermi level. Dashed line gives the trends of the resonance frequency of plasmons free from interaction with the phonons. Dotted lines indicate the two surface polar phonons of SiO_2, ω_{sp1} and ω_{sp2}.

substrate phonons asymptotically approach to the phonon frequencies. This observation indicates that the plasmon resonance frequencies are limited by the substrate phonons, particularly for those in the proximity of phonon energy.

To quantitatively investigate the hybridization of coplanar plasmon modes on polar substrate, e.g., SiO_2, we measured the extinction of GNRAs of a given ribbon width but at varying inter-ribbon distances (see **Figure 3**a). Their extinction spectra are shown in Figure 3b. Each series of the plasmon resonance peaks shifted to the low energy as the filling factor of graphene increased, thus providing a direct evidence of plasmon hybridization in graphene nanostructures. The plasmon coupling behavior can be explained by the dipole-dipole interaction mechanism. All three peaks in an extinction spectrum of a GNRA were caused by the first order excitation modes, which behaved like oscillating dipoles in each graphene nanoribbon. As the inter-ribbon distance deceases, the interaction strength of neighboring dipoles increased, weakening the restoring force of the oscillating charges in each strips, and resulting in lower oscillation frequency of plasmons in the GNRAs. In addition, when the filling factor of graphene increased, more nanoribbons were exposed to the illuminating light spot, thus the extinction amplitudes of all the three peaks increased.

The resonance frequency of the GNRAs with varying inter-ribbon distance is shown in Figure 3c. The finite-element simulated curve corresponding to peak 3 is also presented (see Method). The simulated curves agree with the trend that shows the down-shift of resonance frequency as the filling factor increases. The peak does not fall below the surface optical phonon of SiO_2, ω_{sp2}, due to the plasmon-phonon interaction (the plasmon cannot survive if its frequency is the same as the substrate phonon[5]. For nonpolar substrate, the plasmon resonance is not limited by any phonon modes; hence the decrease of the resonance frequency should be larger than that for a polar substrate. The resonance frequencies of GNRA in free space and on silicon were both calculated to stress the substrate effect, shown in Figure 3c. The decreasing rate of the resonance frequency on a nonpolar substrate is much faster than that on the polar SiO_2 substrate, especially for large filling factors of graphene.

The coupling strength can be quantified through the shift of resonance frequency relative to the weak coupling limit (when the inter-ribbon spacing is large and the modes hybridization can be ignored). Figure 3d shows the calculated coupling strength of plasmons in GNRAs on various substrates. The coupling strength is small (less than ~0.05) for the polar SiO_2 substrate. In contrast, for nonpolar substrates, the coupling strength increases exponentially as the filling factor of graphene increases. For free-standing GNRAs and those on silicon substrate, the interaction shifted the plasmon resonance frequency over 10%, when the filling factor is greater than 2/3 (gap-to-ribbon ratio equal to 0.5). Note that the coupling strength only weekly depends on the ribbon width and the Fermi level.

Because the plasmons on nonpolar substrate are free from interaction with substrate phonons, they are more suitable for broadband electro-optical applications.[12,15] However the hybridization of the coplanar plasmons is also much more stronger than that of the plasmons on polar substrate, which is a disadvantage for the integration of plasmonic nanostructures. Hence, the plasmon coupling in neighboring graphene nanostructures should be effectively reduced to enhance the integratability of the system.

An intuitive and convenient approach to achieve this is to build noble metal fins between adjacent graphene structures. Noble metals are perfect electric conductors in the infrared frequency range, resulting in nearly zero penetration of electromagnetic field in the metal and thereby eliminating the hybridization of modes from neighboring graphene strips. The evanescent fields of plasmons are confined in the spaces defined by the inserted metal walls. The height of the metal

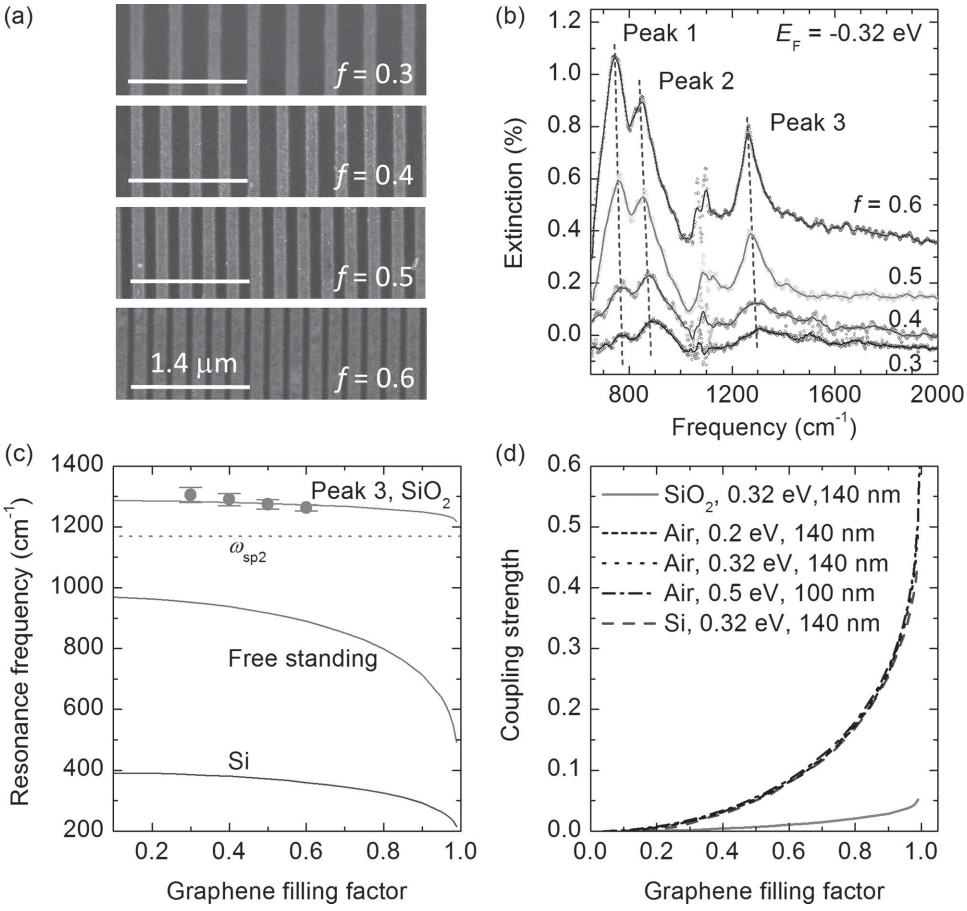

Figure 3. (a) SEM images of GNRAs with filling factors of 0.3, 0.4, 0.5 and 0.6, respectively. The nanoribbon widths were 140 nm. (b) Extinction spectra of GNRAs shown in (a) obtained at the Fermi level of -0.32 eV. (c) Resonance frequency of Peak 3 extracted from (b) with respect to graphene filling factor. Solid lines show the simulated resonance frequency of the GNRAs on various substrates (SiO_2, Si and free standing). The surface polar phonon ω_{sp2} is indicated by the dotted line. (d) Coupling strength of GNRAs with different ribbon widths, under different Fermi levels and on various substrates as a function of graphene filling factor.

fins does not influence the plasmon confinement and the resonance frequency, as long as the majority of the energy of the individual plasmon is confined between the two metal fins. However, our calculation showed that the plasmon resonance frequency exhibits a slight red-shift due to the increased mode confinement. For instance, the extinction maximum of the graphene ribbon array with width of 140 nm and filling factor of 0.5, shifts ~7 cm^{-1} to the lower frequency in the presence of silver walls with 20 nm width, as shown in **Figure 4**a. Here we assumed that graphene structures were placed on a nonpolar substrate with permittivity of 2.11, which is the high frequency limit permittivity of silica.

The shift of plasmon resonance caused by the inserted metal walls can be offset by engineering the dielectric environment in the proximity of graphene ribbons. In principal, a stable electromagnetic resonances in a optical cavity blue shifts with decreasing optical length of the cavity. Thus a decreasing of the average permittivity between two adjacent metal fins will cause an increased resonance frequency of graphene plasmons. For instance, when two air grooves of 60 nm width are present beside each silver wall, the resonance frequency shifts to ~780 cm^{-1}, which represents the situation of the weak coupling limit. The resonance frequency can be tuned for more than 40 cm^{-1} by varying the air groove width (Figure 4b). The near field intensities of the plasmon modes between two silver fins (120 nm height) with and without air grooves are shown in the inset of Figure 4b. The distributions of the mode intensities exhibit similar characteristics. Like in a GNRA without metal fins, the ribbon edges concentrate electromagnetic energy. For both configurations, the resonance modes are confined between the two metal fins, thus preventing a hybridization of the coplanar plasmons. When air grooves are engineered, more energy spreads to the low-permittivity region, resulting in an up-shifted resonance frequency. Note that inserting metal-air heterostructures in GNRAs does not change the damping behavior of the plasmon resonances, as suggested by the nearly unchanged peak width in the extinction spectra (Figure 4a).

3. Conclusion

The hybridization of the plasmons in graphene nanoribbon arrays increases exponentially as the separation between

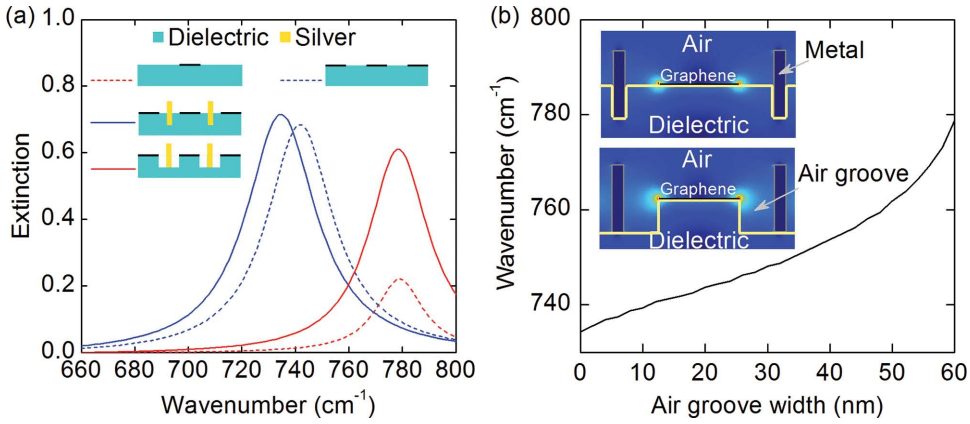

Figure 4. (a) Extinction spectra of the four configurations shown in the inset. The ribbon width of graphene is 140 nm; graphene filling factor is 0.5; silver wall width is 20 nm; air groove width is 60 nm. (b) Resonance frequency of GNRAs with metal-air structures as a function of the air groove width. Insets display the near field power densities of the resonance modes with air groove width of 0 (no air grooves) and 60 nm.

graphene nanostructures decreases, as revealed by far-field infrared spectroscopy. The coupling strength is nearly independent on the carrier concentrations and the ribbon width of graphene, but highly affected by the substrate material. Our experimental and theoretical results indicated that the plasmon coupling strength on nonpolar substrate is much greater than that on polar substrate. Finally, we introduce a rationally designed metal-dielectric heterostructure that effectively reduces the interference between neighboring plasmon modes. Our study presents a scheme for high-density on-chip integration of graphene-based plasmonic circuits.

4. Experimental Section

Preparation of Graphene: Large-area graphene was grown by chemical vapor deposition on copper and then transferred to a SiO_2/Si wafer using poly(methyl methacrylate) (PMMA) assisted wet-transfer techniques.[27,28] Before the transfer process, a PMMA layer was spin-coated on the upside of graphene/copper foil. Subsequently, the backside graphene was removed using oxygen plasma and the copper foil was selectively etched in 1:1 iron chloride (0.5 mol/L) and hydrochlric acid (0.5 mol/L) solution. The PMMA/graphene film floating on the etchant was cleaned by deionized water several times to rinse the etchant residue and then transferred onto doped Si wafers with 285 nm SiO_2. The chip was left to dry and then the PMMA layer was dissolved by acetone and the whole chip is cleaned by isopropyl alcohol.

Device Fabrication: Nanoribbon arrays were patterned in the graphene by using 100 keV electron beam lithography (Vistec, EBPG5000+) on ~260 nm thick 495 PMMA (MicroChem). The exposed PMMA was developed in 3:1 isopropanol: methyl isobutyl ketone (MIBK) for 1.5 min, and then the graphene exposed to air was etched away using oxygen plasma at 5 Pa and 100 W for 8 s. A second electron beam lithography process was carried out to define the electrode pattern. Devices were then fabricated with contact metal (50 nm-Au/2 nm-Ti) deposition through electron beam evaporation and following a standard metal lift-off technique.

Characterization: The Raman spectra of graphene were all acquired using a micro-Raman microscope (Horiba JobinYvon, LabRAM HR800) with an excitation laser wavelength of 532 nm and a spot size of ca. 1 μm. The morphology of as prepared graphene nanoribbons were characterized by AFM (Bruker, Dimension Icon) using tapping mode and SEM (Hitachi, S-4800) operated at 1 kV. Electrical transport properties at room temperature were characterized with a semiconductor parameter analyzer (Agilent, 4294A). Then the Dirac point of each device was confirmed by the transfer characteristic which was repeated several times.

IR Measurement: The infrared transmission measurements of the devices were performed with a Fourier transform infrared spectrometer with a microscopy (ThermoFisher, Nicolet iN10). The extinction spectra of graphene nanoribbons at the charge neutral point were taken as background and then the extinction spectra of nanoribbons in the same area but at different gate voltages were acquire by automatically subtracting the background. The size range infrared microscope studied was from about 20 to 200 μm in this study. Each measurement was repeated several times to confirm the extinction spectrum. All measurements were performed at room temperature and atmospheric environment.

Simulation Methods: The plasmonic responses of the devices are simulated by the finite element method. The terahertz incident lights impinge perpendicularly on GNRAs. The graphene is modeled as a material with a finite thickness and a phenomenological equivalent permittivity. In our simulations, the graphene thickness (t_g) is set to be 1 nm, at which value the calculations reach proper convergence. The equivalent relative permittivity is derived from the two-dimensional conductivity of graphene and is given by $\varepsilon_g = i\sigma/\varepsilon_0\omega t_g$.[29] Here, ε_0 is the free space permittivity, ω is the light angular frequency, and σ is the graphene conductivity calculated from the Kubo formula.[30] The permittivities of silica, silicon and silver are cited from Palik.[31]

Supporting Information

Supporting Information is available from the Wiley Online Library or from the author.

Acknowledgements

This work is supported by the National Natural Science Foundation of China (No. 51372045). Xiaoxia Yang and Xiang-Tian Kong contributed equally to this work.

[1] P. Avouris, M. Freitag, *IEEE J. Sel. Top. Quan. Electron.* **2014**, *20*, 6000112.
[2] F. H. L. Koppens, D. E. Chang, F. J. Garcia de Abajo, *Nano Lett.* **2011**, *11*, 3370.
[3] W. Gao, G. Shi, Z. Jin, J. Shu, Q. Zhang, R. Vajtai, P. M. Ajayan, J. Kono, Q Xu, *Nano Lett.* **2013**, *13*, 3698.
[4] L. Ju, B. Geng, J. Horng, C. Girit, M. Martin, Z. Hao, H. A. Bechtel, X. Liang, A. Zettl, Y. R. Shen, F. Wang. *Nat. Nanotechnol.* **2011**, *6*, 630.
[5] H. Yan, T. Low, W. Zhu, Y. Wu, M. Freitag, X. Li, F. Guinea, P. Avouris, F. Xia, *Nat. Photonics* **2013**, *7*, 394.
[6] Z. Fang, S. Thongrattanasiri, A. Schlather, Z. Liu, L. Ma, Y. Wang, P. M. Ajayan, P. Nordlander, N. J. Halas, F. J. Garcia de Abajo, *ACS Nano* **2013**, *7*, 2388.
[7] F. Wang, Y. Zhang, C. Tian, C. Girit, A. Zettl, M. Crommie, Y. R. Shen, *Science* **2008**, *320*, 206.
[8] S. H. Lee, M. Choi, T.-T. Kim, S. Lee, M. Liu, X. Yin, H. K. Choi, S. S. Lee, C.-G. Choi, S.-Y. Choi, X. Zhang, B. Min, *Nat. Mater.* **2012**, *11*, 936.
[9] B. Sensale-Rodriguez, *Appl. Phys. Lett.* **2013**, *103*, 123109.
[10] E. H. Hwang, S. Das Sarma, *Phys. Rev. B* **2007**, *75*, 205418.
[11] W. Gao, J. Shu, C. Qiu, Q. Xu, *ACS Nano* **2012**, *6*, 7806.
[12] P. Li, T. Taubner, *ACS Nano* **2012**, *6*, 10107.
[13] A. Andryieuski, A. V. Lavrinenko, *Opt. Express* **2013**, *21*, 9144.
[14] V. W. Brar, M. S. Jang, M. Sherrott, J. J. Lopez, H. A. Atwater, *Nano Lett.* **2013**, *13*, 2541.
[15] Q. Bao, K. P. Loh, *ACS Nano* **2012**, *6*, 3677.
[16] F. Xia, H. Yan, P. Avouris, *Proc. IEEE* **2013**, *101*, 1717.
[17] R. Zia, M. D. Selker, P. B. Catrysse, M. L. Brongersma, *J. Opt. Soc. Am. A* **2004**, *21*, 2442.
[18] A. Y. Nikitin, F. Guinea, F. J. Garcia-Vidal, L. Martin-Moreno, *Phys. Rev. B* **2012**, *85*, 081405.
[19] J. Christensen, A. Manjavacas, S. Thongrattanasiri, F. H. L. Koppens, F. J. Garcia de Abajo, *ACS Nano* **2012**, *6*, 431.
[20] J. H. Strait, P. Nene, W.-M. Chan, C. Manolatou, S. Tiwari, F. Rana, J. W. Kevek, P. L. McEuen, *Phys. Rev. B* **2013**, *87*, 241410.
[21] S. A. Maier, P. G. Kik, H. A. Atwater, S. Meltzer, E. Harel, B. E. Koel, A. A. G. Requicha, *Nat. Materials* **2003**, *2*, 229.
[22] K. S. Novoselov, A. K. Geim, S. V. Morozov, D. Jiang, M. I. Katsnelson, I. V. Grigorieva, S. V. Dubonos, A. A. Firsov, *Nature* **2005**, *438*, 197.
[23] A. Kucirkova, K. Navratil, *Appl. Spectrosc.* **1994**, *48*, 113.
[24] E. H. Hwang, Rajdeep Sensarma, S. Das Sarma, *Phys. Rev. B* **2010**, *82*, 195406.
[25] E. H. Hwang, S. Das Sarma, *Phys. Rev. B* **2009**, *80*, 205405.
[26] M. Jablan, M. Soljacic, H. Buljan, *Phys. Rev. B* **2011**, *83*, 161409.
[27] X. Li, W. Cai, J. An, S. Kim, J. Nah, D. Yang, R. Piner, A. Velamakanni, I. Jung, E. Tutuc, S. K. Banerjee, L. Colombo, R. S. Ruoff, *Science* **2009**, *324*, 1312.
[28] X. Li, Y. Zhu, W. Cai, M. Borysiak, B. Han, D. Chen, R. D. Piner, L. Colombo, R. S. Ruoff, *Nano Lett.* **2009**, *9*, 4359.
[29] A. Vakil, N. Engheta, *Science* **2011**, *332*, 1291.
[30] V. P. Gusynin, S. G. Sharapov, J. P. Carbotte, *J. Phys. Condens. Matter* **2007**, *19*, 026222.
[31] E. D. Palik, *Handbook of Optical Constants of Solids*, Academic Press, London **1985**.

Received: February 25, 2014
Revised: August 17, 2014
Published online: October 1, 2014